Variation in chemical composition and volatility of oxygenated organic aerosol in different rural, urban, and remote environments

Wei Huang[1], Cheng Wu[2,3], Linyu Gao[4], Yvette Gramlich[2,5], Sophie L. Haslett[2,5], Joel
Thornton[6], Felipe D. Lopez-Hilfiker[7], Ben H. Lee[6], Junwei Song[4], Harald Saathoff[4], Xiaoli
Shen[4,8], Ramakrishna Ramisetty[4,9], Sachchida N. Tripathi[10], Dilip Ganguly[11], Feng Jiang[4],
Magdalena Vallon[4], Siegfried Schobesberger[12], Taina Yli-Juuti[12], Claudia Mohr[2,5,13,*]

[1]Institute for Atmospheric and Earth System Research / Physics, Faculty of Science, University of Helsinki, 00014,
Helsinki, Finland

[2]Department of Environmental Science, Stockholm University, 11418, Stockholm, Sweden

[3]Now at: Department of Chemistry and Molecular Biology, University of Gothenburg, 41296, Gothenburg,
Sweden

[4]Institute of Meteorology and Climate Research, Karlsruhe Institute of Technology, 76344, Eggenstein-
Leopoldshafen, Germany

[5]Bolin Centre for Climate Research, Stockholm University, 11418, Stockholm, Sweden

[6]Department of Atmospheric Sciences, University of Washington Seattle, Washington 98195, United States

[7]Tofwerk AG, 3600 Thun, Switzerland

[8]Now at: Department of Earth, Atmospheric, and Planetary Sciences, Purdue University, West Lafayette, Indiana
47907, United States

[9]Now at: TSI Instruments India Private Limited, 560102, Bangalore, India

[10]Department of Civil Engineering, Indian Institute of Technology Kanpur, 208016, Kanpur, India

[11]Centre for Atmospheric Sciences, Indian Institute of Technology Delhi, 110016, New Delhi, India

[12]Department of Technical Physics, University of Eastern Finland, 70211, Kuopio, Finland

[13]Now at: Department of Environmental System Science, ETH Zurich and Laboratory of Atmospheric Chemistry,
Paul Scherrer Institute, 5232 Villigen, Switzerland

Correspondence to: Claudia Mohr (claudia.mohr@psi.ch)

Abstract. The apparent volatility of atmospheric organic aerosol (OA) particles is determined by their chemical composition and environmental conditions (e.g., ambient temperature). A quantitative, experimental assessment

30   of volatility and the respective importance of these two factors remains challenging, especially in ambient measurements. We present molecular composition and volatility of oxygenated OA (OOA) particles in different rural, urban, and remote environments across the globe (including Chacaltaya, Bolivia; Alabama, U.S.; Hyytiälä, Finland; Stuttgart and Karlsruhe, Germany; and Delhi, India) based on deployments of a filter inlet for gases and aerosols coupled to a high-resolution time-of-flight chemical ionization mass spectrometer (FIGAERO-

35   CIMS). We find on average larger carbon numbers (nC) and lower oxygen-to-carbon (O:C) ratios at the urban sites (nC: 9.8±0.7; O:C: 0.76±0.03; average ± 1 standard deviation), compared to the rural (nC: 8.8±0.6; O:C: 0.80±0.05) and remote mountain stations (nC: 8.1±0.8; O:C: 0.91±0.07), indicative of different emission sources and chemistry. Compounds containing only carbon, hydrogen, and oxygen atoms (CHO) contribute highest to the total OOA mass at the rural sites (79.9±5.2%), in accordance with their proximity to forested areas (66.2±5.5% at the

40   mountain sites and 72.6±4.3% at the urban sites). The largest contribution of nitrogen-containing compounds (CHON) are found at the urban stations (27.1±4.3%), consistent with their higher NO_x levels. Besides, we parametrize OOA volatility (saturation mass concentrations, C_{sat}) using molecular composition information and compare it with the bulk apparent volatility derived from thermal desorption of the OOA particles within the FIGAERO. We find differences in C_{sat} values of up to ~3 orders of magnitude, and variation in thermal desorption

45   profiles (thermograms) across different locations and systems. From our study, we draw the general conclusion that environmental conditions (e.g., ambient temperature) do not directly affect OOA apparent volatility, but rather indirectly by influencing the sources and chemistry of the environment and thus the chemical composition. The comprehensive global dataset provides results that show the complex thermodynamics and chemistry of OOA and their changes during its lifetime in the atmosphere, and that generally the chemical description of OOA suffices to

50   predict its apparent volatility, at least qualitatively. Our study thus provides new insights that will help guide choices of e.g. descriptions of OOA volatility in different model frameworks which has been previously simplified due to challenges to measure and represent it in models.

1 Introduction

Chemical composition and volatility of atmospheric organic aerosol (OA) particles are interconnected.

55   Functionalization of organic molecules can modify their vapor pressure by several orders of magnitude (Pankow and Asher, 2008;Donahue et al., 2011;Graham et al., 2022;Isaacman-VanWertz and Aumont, 2021;Kroll and Seinfeld, 2008). Volatility determines whether a compound partitions into or evaporates from the particle phase and thus influences particulate mass and lifetime in the atmosphere. Accurate predictions of atmospheric organic particle mass thus require a quantitative understanding of the chemical nature and volatility of its components.

60   This is of special importance for oxygenated organic aerosol (OOA), most of which is of secondary origin (i.e., SOA) (Jimenez et al., 2009) and involves phase transitions and chemical reactions in all phases. Further, the conditions of the atmosphere, e.g., temperature, play a critical role. A semi-volatile compound may be in the gas phase in the boundary layer at 25 °C but condense at an altitude of ~4.5 km where the ambient temperature is ~20 °C lower, and consequently its apparent volatility is lower by up to ~2 orders of magnitude (Bardakov et al.,

65   2021;Donahue et al., 2011;Epstein et al., 2010;Stolzenburg et al., 2018). The complex thermodynamics and chemistry of OOA and their changes during its lifetime in the atmosphere are challenging to measure and represent

in modelling frameworks, resulting in simplified descriptions of volatility (Nozière et al., 2015;Hallquist et al., 2009).

The development of the filter inlet for gases and aerosols coupled to a time-of-flight chemical ionization mass spectrometer (FIGAERO-CIMS) has enabled the combined analysis of molecular composition and volatility of OOA particles in near-real time (Thornton et al., 2020;Lopez-Hilfiker et al., 2014). OOA volatility can be derived in two ways from the FIGAERO-CIMS:

1) The molecular information of OOA can be used to parametrize volatility via calculations of the effective saturation mass concentrations (C_{sat}) of different organic compounds (Donahue et al., 2011;Li et al., 2016;Mohr et al., 2019;Isaacman-VanWertz and Aumont, 2021;Graham et al., 2022). There are various parametrization methods to calculate C_{sat}, based on different assumptions, training datasets, or structure-based estimation methods (Isaacman-VanWertz and Aumont, 2021). However, calculated C_{sat} from different parametrizations may vary among each other: while modified Li method (Li et al., 2016;Isaacman-VanWertz and Aumont, 2021) tends to estimate higher vapor pressures than expected for low-volatility species, Daumit method (Daumit et al., 2013) and Donahue method (Donahue et al., 2011) (also the updated Mohr method (Mohr et al., 2019)) are found to estimate lower vapor pressures (Isaacman-VanWertz and Aumont, 2021). The discrepancy in C_{sat} among different parametrizations can span several orders of magnitude and become even larger for compounds with increasing nitrogen numbers, especially for organonitrates with multiple nitrate groups (Wu et al., 2021;Isaacman-VanWertz and Aumont, 2021;Graham et al., 2022). This could induce uncertainties associated with volatility estimates particularly for complex ambient particle matrix (O'Meara et al., 2014).

2) While the particles are thermally desorbed within the FIGAERO for molecular composition analysis with CIMS, the instrument also yields a qualitative measure of particle volatility through the signal evolution as a function of desorption temperature (i.e., thermograms) (Lopez-Hilfiker et al., 2014;Lopez-Hilfiker et al., 2015). A model framework has also been developed to reproduce the shape of thermograms (Schobesberger et al., 2018). The desorption temperature at which a compound exhibits maximum signal (T_{max}) correlates with the compound's enthalpy of sublimation and can be used to infer its saturation vapor pressure (Lopez-Hilfiker et al., 2015;Mohr et al., 2017). Evaporative behavior, and hence thermogram shape, T_{max} and inferred volatility of a particle-bound compound are subject to artefacts from thermal decomposition (Lopez-Hilfiker et al., 2015;Yang et al., 2021), heating rate (Yang et al., 2021;Ylisirniö et al., 2021;Thornton et al., 2020;Schobesberger et al., 2018), FIGAERO geometry (Ylisirniö et al., 2021), the presence of isomers (Thompson et al., 2017;Masoud and Ruiz, 2021), and particle-phase diffusivity and viscosity (Yli-Juuti et al., 2017;Huang et al., 2018). As a consequence, thermogram shape and T_{max} for an individual compound can vary among different chamber studies (D'Ambro et al., 2017;Huang et al., 2018;Wang and Ruiz, 2018) and field measurements (Thompson et al., 2017;Huang et al., 2019b;Gaston et al., 2016), which could also induce uncertainties associated with volatility estimates, similar to parametrization methods.

Overall, the relationship between molecular composition-derived volatility and thermal-desorption-derived volatility is not always straight forward given the rather large uncertainties of both methods (Isaacman-VanWertz and Aumont, 2021;Voliotis et al., 2021;Masoud and Ruiz, 2021;Wu et al., 2021). Huang et al. (2019b) found consistent results of bulk volatility for OOA particles measured in Stuttgart, Germany, when using volatility parametrizations and thermograms, indicative of the connection between chemical composition and volatility. Wu et al. (2021) found a qualitative agreement between T_{max} and C_{sat} for individual compounds of SOA particles in their chamber studies, but varying results for the bulk volatility when using different parametrizations and

thermograms. Further comprehensive investigations of the relationship between volatility and chemical composition of OOA particles are warranted, particularly for ambient measurements.

110   In this study, we present an overview of the chemical composition of OOA and OOA volatility derived from both molecular composition measurements and thermogram analyses for a number of ambient FIGAERO-CIMS datasets across the globe (Chacaltaya, Bolivia; Alabama, U.S.; Hyytiälä, Finland; Stuttgart and Karlsruhe, Germany; Delhi, India). We assess how different environments (e.g., emission sources and meteorological parameters) influence the particle chemical composition and volatility derived from these two methods, discuss

115   the reasons for differences and similarities, and the relationship between volatility and chemical composition for the different locations.

2 Methodology

2.1 Measurement sites

The measurement sites of this study are listed in Table 1. The list includes one remote mountain site (MCC,

120   16°21'00.0" S, 68°07'48.0" W), located at the GAW (Global Atmosphere Watch) high altitude research station Chacaltaya (~5240 m a.s.l.), ~25 km northeast of La Paz city (~3640 m a.s.l.), Bolivia (Bianchi et al., 2022); three rural sites, the first one located in the Rhine river valley near Eggenstein-Leopoldshafen, ~12 km north of the city of Karlsruhe, Germany (REL, 49°6′10.54″ N, 8°24′26.07″ E) (Huang et al., 2019a), the second one in the boreal forest of Hyytiälä, Finland (RHT, 61°50'47.2" N, 24°17'43.3" E) (Mohr et al., 2017;Mohr et al., 2019), and the

125   third one located near Centreville, Alabama, United States (RAB, 33°10'48.0" N, 86°46'48.0" W) (Lopez-Hilfiker et al., 2016); and three urban sites, the first one located in a park in the city of Stuttgart, Germany (UST, 48°47′55.1" N, 9°12′13.5" E) (Huang et al., 2019b); the second one right next to a road crossing the city center of Karlsruhe, Germany (UKA, 49°00'35.0" N, 8°25'02.8" E), and the third one on a university campus in the city of Delhi, India (UDL, 28°32'48.8" N, 77°011'26.8" E). For MCC, UST, and UKA, measurements from different

130   seasons were included to investigate the influence of seasonal variation in emission sources and/or chemistry on OOA composition and volatility. The campaign-average values for co-located measurements of meteorological parameters (temperature (T) and relative humidity (RH)), trace gases (O_3, NO_2, and SO_2), equivalent black carbon (eBC), and total non-refractory particulate mass are listed in Table S1.

135   **Table 1.** Overview of the measurement sites included in this study, their locations, and the measurement periods.

Abbreviation	Location	Measurement period	Description
MCC	Chacaltaya, Bolivia	April 9-26, 2018 (transition season); May 7-June 2, 2018 (dry season)	Mountain site
REL	near Eggenstein-Leopoldshafen, Germany	August 18-Sept. 1, 2016	Rural site
RAB	near Centreville, Alabama, U.S.	June 4-July 16, 2013	Rural site
RHT	Hyytiälä, Finland	April 11-June 3, 2014	Rural site
UST	Stuttgart, Germany	July 5-August 17, 2017 (summer); February 5-March 5, 2018 (winter)	Urban background site
UKA	Karlsruhe, Germany	June 28-July 29, 2019 (summer); February 22-March 30, 2020 (winter)	Urban curb site
UDL	Delhi, India	January 11-February 5, 2019	Urban background site

2.2 Measurements and volatility determination of OOA particles

2.2.1 Measurements of OOA particles

Particulate oxygenated organic compounds were measured with a FIGAERO-CIMS (Aerodyne Research Inc. or from the University of Washington (Lopez-Hilfiker et al., 2014)) using iodide (I⁻) as the reagent ion. Iodide-CIMS

140   is sensitive to more polar oxygenated organic compounds with three to eight oxygen atoms (Lee et al., 2014;Riva et al., 2019;Huang et al., 2019a). Inlet flow and residence time, particle deposition time, mass loadings on the filter, and instrumental parameters for the different campaigns are summarized in Table S2. Differences in instrumental parameters such as IMR (ion molecule reaction chamber) pressure, ion source, the ratio of sample and ionizer flow, and the voltage settings of the mass spectrometer can affect the sensitivities of organic compounds and therefore

145   their measured distribution. Here we simply use mass fractions of compounds calculated using sensitivities assumed or assessed for the individual campaigns/instruments, since the focus of this study is not to report and compare absolute mass concentrations of OOA at different locations. An in-depth analysis of the differences in instrumental parameters among different campaigns, and how they affect the measured OOA composition, is beyond the scope of this paper. Data were analyzed with the software packages "tofTools" (developed by Junninen

150   et al. (Junninen et al., 2010)) or "Tofware" (provided by Tofwerk Ltd.).

For REL, RHT, RAB, MCC, and UDL, aerosol particles were measured in-situ with the FIGAERO-CIMS (Huang et al., 2018;Mohr et al., 2019;Lopez-Hilfiker et al., 2016;Bianchi et al., 2022). Particle-phase backgrounds were assessed in regular intervals by placing an additional Teflon (Polytetrafluoroethylene, PTFE) filter upstream of the normal filter and using the same deposition procedure as for the ambient measurements. These data were

155   then used for background subtraction.

For UST and UKA, aerosol particles were deposited on Teflon filters and analyzed later in the laboratory with FIGAERO-CIMS ("offline mode"; see Table S2) (Huang et al., 2019b;Cai et al., 2023). Filters were kept frozen until analysis. Deposition times were varied (see Table S2) based on ambient organic mass concentrations measured by a concurrent high-resolution time-of-flight aerosol mass spectrometer (HR-ToF-AMS, Aerodyne

160 Research Inc.) in order to achieve similar organic mass loadings on the filter and to avoid mass loading effects
(Huang et al., 2018;Wang and Ruiz, 2018). A total of 21 (10) and 29 (23) filter samples were collected in summer
(winter) at UST and UKA, respectively. Particle-phase backgrounds were assessed by placing prebaked clean
filters in the filter holder at the measurement sites with the deposition flow switched off. These field blank samples
were also analyzed by FIGAERO-CIMS in the laboratory like the samples and used for background subtraction.

165 **2.2.2 Volatility determination of OOA particles**

OOA volatility was determined for all sites based on FIGAERO-CIMS thermograms and C_{sat} parametrizations.
Different temperature ramp rates affect T_{max} (Schobesberger et al., 2018;Yang et al., 2021;Ylisirniö et al.,
2021;Thornton et al., 2020). The ramp rates for all measurements shown here varied between 6.7 and 13.3 °C/min
(see Table S2), inducing a T_{max} difference of up to 5 °C (Schobesberger et al., 2018;Ylisirniö et al., 2021;Thornton
170 et al., 2020). Since for most locations no calibrations of the relationship between T_{max} and C_{sat} are available (Wang
et al., 2020;Ylisirniö et al., 2021), we present and discuss here only relative variations in themrogram shapes and
T_{max}, including the variations caused by different ramp rates, and compare them qualitatively to the variation in
C_{sat} determined from parametrization.

C_{sat} (298 K) was calculated for all sites using the approach by Li et al. (2016) as in equation (1):

175 $$\log_{10} C_{sat} (298\,\text{K}) = (n_C^0 - n_C) \times b_C - n_O \times b_O - 2 \times \frac{n_C \times n_O}{(n_C + n_O)} \times b_{CO} - n_N \times b_N - n_S \times b_S \qquad (1)$$

where n_C, n_O, n_N, and n_S are the number of carbon, oxygen, nitrogen, and sulfur atoms in the organic compound,
respectively; n_C^0 is the reference carbon number; b_C, b_O, b_N, and b_S are the contribution of each atom to $\log_{10} C_{sat}$,
respectively; b_{CO} is the carbon–oxygen nonideality (Donahue et al., 2011). Since the empirical approach by Li et
al. (2016) was derived with very few organonitrates, we modified the C_{sat} (298 K) of CHON compounds by treating
180 all NO_3 groups like OH groups following the approach by Daumit et al. (Daumit et al., 2013;Isaacman-VanWertz
and Aumont, 2021). A recent study however found that the parametrization of C_{sat} for nitrate groups is highly
uncertain (Graham et al., 2022).

We also adjusted the C_{sat} (298 K) to the measured ambient temperature, C_{sat} (T), using the approach by Donahue
et al. (2011) and Epstein et al. (2010) as in equations (2) and (3):

185 $$\log_{10} C_{sat} (T) = \log_{10} C_{sat} (298\,\text{K}) + \frac{\Delta H_{vap}}{R\ln(10)} \times \left(\frac{1}{298} - \frac{1}{T}\right), \qquad (2)$$

$$\Delta H_{vap}(\text{kJ mol}^{-1}) = -11 \times \log_{10} C_{sat} (298\,\text{K}) + 129 \qquad (3)$$

where T is the temperature in Kelvin; C_{sat} (298 K) is the saturation mass concentration at 298 K; ΔH_{vap} is the
vaporization enthalpy; and R is the gas constant (8.3143 J K^{-1} mol^{-1}).

3 Results and discussion

190 **3.1 Bulk molecular composition of OOA particles**

3.1.1 Average number of carbon and oxygen atoms and oxygen-to-carbon ratios

We focus our analysis of the bulk molecular composition of OOA from the different locations here on the average number of carbon (nC) and oxygen atoms (nO) as they affect the parametrized C_{sat}, and also could be used to indicate precursor sources (Huang et al., 2019a) and oxidation processes, respectively. Figure 1a shows the average

195   mass-weighted nO vs. nC for all compounds with the molecular formula $C_{x\geq1}H_{y\geq1}O_{z\geq1}X_{0-n}$ (CHOX; X are different atoms such as N, S, Cl, or a combination thereof) measured by FIGAERO-CIMS for each campaign. The markers are color-coded by the average mass-weighted oxygen-to-carbon (O:C) ratios. The observed average nC and nO range from 7.7 to 11.2 and from 4.9 to 7.1, respectively. There is an overall trend of increasing nO with increasing nC (Figure 1a), with the spring-time OOA at the rural station Hyytiälä, Finland (RHT), and the wintertime OOA

200   at the urban station Delhi, India (UDL) deviating from that general trend (see discussions below). The overall trend shows the effect of the length of carbon backbone on the number of potential oxygen atoms that can be added to the carbon chain (Huang et al., 2019a).

Generally, at the urban sites, OOA particles exhibit on average larger nC (9.8±0.7; average ± 1 standard deviation) compared to the rural (8.8±0.6) and mountain stations (8.1±0.8), indicative of different emission sources

205   and OOA precursors (Huang et al., 2019b).

At the remote mountain site Chacaltaya, Bolivia, OOA has a relatively longer carbon backbone (nC: 8.4±0.8) in the transition season (MCC-t) than in the dry season (MCC-d, nC: 7.7±0.7). While air masses arriving at Chacaltaya during the dry season are more affected by the anthropogenic sources, air masses reaching Chacaltaya during the transition season have more influence from the Amazon Basin (Aliaga et al., 2021;Zha et al., 2023b),

210   and hence a higher contribution of monoterpene ($C_{10}H_{16}$) and especially isoprene (C_5H_8) oxidation products are expected (also reflected in the clear peak of C_5 compounds in Figure S1) (Zha et al., 2023a).

Rural Alabama in U.S. (RAB) and rural Hyytiälä in Finland (RHT), which are both forested stations albeit in different biomes, show respective OOA composition with nC of 8.0±0.4 at RAB and 9.1±0.6 at RHT. This is likely due to the different distributions of terpene emissions with more isoprene at RAB (Lopez-Hilfiker et al., 2016;Lee

215   et al., 2016) and mostly monoterpenes at RHT (Li et al., 2020;Huang et al., 2021). It is also seen in the higher contributions of C_{8-10} compounds for RHT, and comparable contributions of C_5 and C_{8-10} compounds for RAB (Zhang et al., 2018) (Figure S1). The third rural site, REL, which is situated at a location with substantial anthropogenic as well as biogenic influence dominated by monoterpene emissions (Huang et al., 2019a), has a comparable nC (9.2±0.8) to RHT and again shows a relatively higher contributions of C_{8-10} compounds (Figure

220   S1).

For the urban sites, the curb site in Karlsruhe, Germany (UKA) has a larger nC (summer: 10.7±0.8; winter: 11.2±0.8) compared to the urban background site in the nearby city of Stuttgart (UST, summer: 8.8±0.4; winter: 8.7±0.9). The nC for wintertime Delhi in India (UDL, 9.4±0.4) is between that of UKA and UST. Such differences are likely due to the UKA and UDL measurement locations being more directly impacted by traffic emissions

225   (Kumar et al., 2022) with higher contributions of larger aromatic compounds (Zheng et al., 2017;Lim et al., 1999). This is substantiated by the observed elevated contributions of C_{11-18} compounds (Figure S1) and higher DBE (double bond equivalent) values (Table S1). In addition, all three urban sites, despite their very different locations, show a similar seasonal pattern, with higher contributions of C_{8-10} compounds in summer from biogenic emissions, and higher contributions of C_6 compounds (e.g., levoglucosan, $C_6H_{10}O_5$) in winter due to biomass burning

230   emissions (Figure S1) (Huang et al., 2019b;Kumar et al., 2022).

Whereas the nC values may give some indication of OOA precursor emission sources, the average nO and O:C ratios are linked to different aging processes and/or varying distance from the sources (Jimenez et al., 2009). The

urban stations exhibit on average the lowest O:C ratios (0.76±0.03), compared to the rural (0.80±0.05) and remote mountain stations (0.91±0.07).

235 OOA particles during the transition season at the mountain site Chacaltaya, Bolivia (MCC-t), have relatively larger nO (6.2±0.3), but slightly lower O:C ratio (0.89±0.08) compared to the dry season (MCC-d; nO: 5.8±0.3; O:C: 0.94±0.05). For two of the rural stations (RAB in the southeastern U.S. and RHT in Finland), nO is comparable (RAB: 5.7±0.2; RHT: 5.7±0.3), but O:C is slightly higher at RAB (0.81±0.04; RHT: 0.77±0.05). This may again be due to the difference in dominating terpene sources (isoprene for RAB (Lopez-Hilfiker et al., 2016) and monoterpenes for RHT (Li et al., 2020); also reflected in Figure S1). The third rural site, REL in Germany (during summertime with substantial anthropogenic and biogenic influence) (Huang et al., 2019a), has higher nO (6.6±0.5) and O:C (0.83±0.06) compared to RAB and RHT, despite the fairly large nC (9.2±0.8). This could be related to more intense photochemistry/oxidation with higher temperature and/or solar radiation at this site (Table S1). Lower temperature and solar radiation could also be the reason for RHT deviating from the general trend of nO and nC in Figure 1a.

The urban sites in Germany (Karlsruhe, UKA, and Stuttgart, UST) have similar nO in summer and in winter (UKA: summer: 7.0±0.4; winter: 7.1±0.4; UST: summer: 6.4±0.2; winter: 6.7±0.2). In comparison, nO for the winter Delhi site (UDL) is 4.9±0.1 due to the dominance of primary OA (Kumar et al., 2022), resulting in its deviation from the general trend of nO and nC (Figure 1a). Besides, O:C ratios are lower for UKA (summer: 0.73±0.02; winter: 0.73±0.04) and UDL (0.66±0.02) compared to UST (summer: 0.82±0.02; winter: 0.89±0.06), which relates back to its larger nC (see Figure 1a) as a result of its high proximity to traffic emissions (Kumar et al., 2022) with more larger aromatic compounds (Lim et al., 1999;Zheng et al., 2017) (see discussions above and Figure S1). Despite the influence of different OOA sources in summer and winter (biogenic emissions vs. biomass burning contributions) for both German urban sites UKA and UST (Huang et al., 2019b), only UST exhibits higher O:C ratios in winter than summer. This could be due to the complex topography of the city of Stuttgart, resulting in stronger surface temperature inversions and consequently longer aging time of air masses (Huang et al., 2019b;Baumbach and Vogt, 2003).
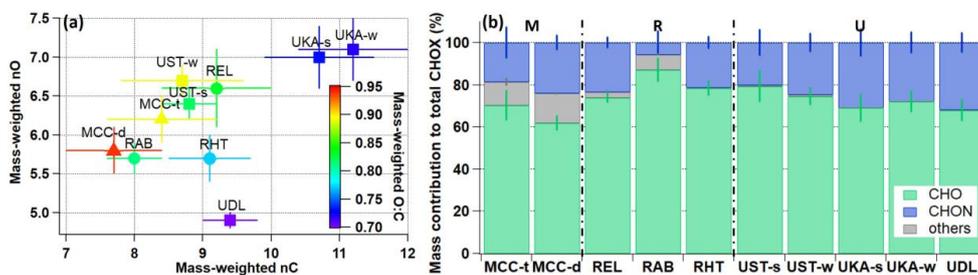
Figure 1. (a) Campaign-average mass-weighted number of oxygen atoms (nO) vs. number of carbon atoms (nC) at the different locations and seasons (Mountain sites in triangles, Rural sites in circles, and Urban sites in squares; for a list of nC and nO values see Table S1), with the markers colored by the corresponding campaign-average mass-weighted oxygen-to-carbon (O:C) ratios; **(b)** Campaign-average mass contributions of organic compounds (separated into CHO, CHON, and other compounds) for the different campaigns (M = mountain sites, R = rural sites, U = urban sites) and seasons (s = summer, w = winter, t = transition, d = dry).

265

3.1.2 Mass contribution of organonitrates

The presence of NO_x during the oxidation of volatile organic compounds (VOC) can lead to the formation of organonitrates, either via reactions with peroxy radicals or formation of NO_3 radicals acting as VOC oxidants, and influence SOA yields and properties of OOA (D'Ambro et al., 2017;Ng et al., 2007;Faxon et al., 2018;Wu et al.,

270 2021). Organonitrates have been found to make up an important fraction of total OA particle mass globally (Kiendler-Scharr et al., 2016;Huang et al., 2019a;Lee et al., 2018). Due to their connection to emissions from fossil fuel burning, they can be indicators of the anthropogenic influence of a particular location. To a lesser extent, also lightning is a source of atmospheric NO_x (Murray, 2016). Here we simply group all organic compounds containing at least one nitrogen atom (CHON) and loosely define them as organonitrates (Lee et al., 2016;Huang et al., 2019a).

275 Compounds containing only carbon, hydrogen, and oxygen atoms are grouped as CHO.

Average mass contributions of CHO and CHON for the different locations are shown in Figure 1b. Overall, CHO compounds clearly dominate the OOA mass at all locations (62.0–87.1%). CHO contributions are on average higher at the rural sites (79.9±5.2%) compared to the mountain (66.2±5.5%) and urban sites (72.6±4.3%), in accordance with their proximity to forested areas. The nitrogen-containing compounds (CHON) contribute 18.7–

280 31.8% to the total OOA mass. A low CHON fraction is observed at the rural station in southeastern U.S. (RAB; 5.6±2.6%), possibly due to the less efficient production rates of CHON and/or their faster loss rates caused by hydrolysis under the high RH there (Table S1) (Lee et al., 2020;Hu et al., 2011;Lee et al., 2016;Pye et al., 2015). As expected, the largest contributions of CHON compounds are found at the urban stations (27.1±4.3%), coinciding with their higher NO_x levels (15.8±8.7 ppbv; Table S1), but overall, differences between stations and

285 seasons are small.

The compounds labelled as "others" in Figure 1b are mostly identified as CHOS or CHONS compounds, making up 0.1–14.1% of the total OOA mass. Sulfur-containing compounds exhibit non-negligible contributions for MCC, REL, and RAB. This is likely due to varying sources for these locations: The mountain site in Bolivia (MCC) was influenced by volcanic emissions during the campaign (Bianchi et al., 2022), the rural sites in central

290 Europe (REL) and southeastern U.S. (RAB) by nearby refineries and/or power plants (Huang et al., 2019a;Fry et al., 2018).

3.2 Volatility of OOA particles

3.2.1 Volatility derived from molecular composition

For each campaign we calculated $C_{sat}(T)$ for each compound based on its molecular composition (see more details

295 in section 2.2.2) (Donahue et al., 2011;Isaacman-VanWertz and Aumont, 2021;Li et al., 2016;Mohr et al., 2019) and grouped all compounds into a 25-bin VBS (volatility basis set; Figure S2) (Donahue et al., 2011;Donahue et al., 2012). The 25 volatility bins were then further aggregated into extremely low-volatile organic compounds (ELVOC, $C_{sat}(T)$ lower than $10^{-4.5}$ µg m^{-3}), low-volatile organic compounds (LVOC, $C_{sat}(T)$ between $10^{-4.5}$ and $10^{-0.5}$ µg m^{-3}), semi-volatile organic compounds (SVOC, $C_{sat}(T)$ between $10^{-0.5}$ and $10^{2.5}$ µg m^{-3}), and

300 intermediate-volatility organic compounds (IVOC, $C_{sat}(T)$ between $10^{2.5}$ and $10^{6.5}$ µg m^{-3}) (Donahue et al., 2009). The average contributions of different volatility groups to total OOA are shown in Figure 2, together with the average mass-weighted $\log_{10}C_{sat}(T)$. Note that the bulk apparent volatility of OOA particles, i.e., average mass-

weighted $\log_{10}C_{sat}$ (T), which represents the overall observed $\log_{10}C_{sat}$ (T) of the OOA as a whole (D'Ambro et al., 2018), is different from the $\log_{10}C_{sat}$ (T) and volatility of the (pure) compounds detected.

305   We find that the more volatile species with C_{sat} (T) between 10^0 and 10^4 µg m^{-3} make up the biggest mass contributions at all locations (47.7–83.8%); LVOC and ELVOC contribute substantially (13.4–42.1%; Figure 2 and S2). In general, the VBS distribution pattern does not seem to have huge differences across different systems and environments, despite that a large (though not all) fraction of OOA can be detected by iodide-CIMS (Riva et al., 2019;Huang et al., 2021). Whereas LVOC and ELVOC may be important for the early stages of atmospheric

310   new particle formation, they certainly do not dominate the OOA mass. Note that thermal decomposition of larger organic compounds during particle desorption with the FIGAERO could contribute, in particular, to the IVOC fraction (Huang et al., 2019b;Lopez-Hilfiker et al., 2016). Resolving and subtracting the thermal decomposition compounds using multi-peak fitting methods (Lutz et al., 2019) or with the help of positive matrix factorization (Buchholz et al., 2020) may, however, introduce uncertainties due to some ambiguity during the implementation

315   and interpretation (Graham et al., 2022;Voliotis et al., 2021). Using the thermal decomposition estimation approach by Wu et al. (2021) the decomposition fraction is estimated to be 5.8–35.9% (see more discussions below), which is close to the reported thermal fragmentation contributions (1–27%) for nitrate SOA in a recent chamber study (Graham et al., 2022). This has however an insignificant effect on the bulk molecular composition of OOA particles, which is e.g. within the corresponding standard deviation range of nC, nO, and O:C ratios.

320   The mountain site in Bolivia exhibits slightly higher contributions from the more volatile species (i.e., IVOC) in the dry season (MCC-d, 31.2±3.9%) compared to the transition season (MCC-t, 20.0±5.0%). Consistently, also the average mass-weighted $\log_{10}C_{sat}$ (T) value is higher for MCC-d (0.58±0.35 µg m^{-3}) than MCC-t (-0.18±0.43 µg m^{-3}). In addition to the higher thermal decomposition contribution for MCC-d (~34.3%) compared to MCC-t (~26.3%), higher contributions of CHON and sulfur-containing organic compounds during the dry season (see also

325   Figure 1b) could also play a role (Peräkylä et al., 2020). Even though the addition of a NO$_3$ functional group is assumed to decrease a compound's vapor pressure by up to several orders of magnitude (Donahue et al., 2011;Graham et al., 2022;Pankow and Asher, 2008), CHON compounds with the same nC and nO as a CHO compound (e.g., $C_{10}H_{15}NO_7$ vs. $C_{10}H_{16}O_7$), are expected to have a higher vapor pressure (Donahue et al., 2011;Lee et al., 2018;Pankow and Asher, 2008). Different origin of air masses and hence atmospheric processing time and

330   chemistry may be another reason for the slight differences in OOA volatility between the seasons (Aliaga et al., 2021;Bianchi et al., 2022).

Among the rural sites in Germany (REL), Finland (RHT), and southeastern U.S. (RAB), RAB shows the highest volatility (IVOC: 49.2±4.9%; ELVOC: 2.4±1.3%; $\log_{10}C_{sat}$ (T): 2.0±0.4 µg m^{-3}) compared to REL (IVOC: 38.8±6.3%; ELVOC: 12.5±5.4%; $\log_{10}C_{sat}$ (T): 0.67±0.67 µg m^{-3}) and RHT (IVOC: 32.7±6.1%; ELVOC:

335   5.5±2.1%; $\log_{10}C_{sat}$ (T): 1.0±0.5 µg m^{-3}). RAB is the southernmost station of all rural sites, with the highest RH (also temperature; Table S1) and high emissions of isoprene, and thus the reactive uptake of IEPOX (isoprene-epoxydiol) in aqueous aerosol is likely a more important SOA pathway compared to REL and RHT. This result again shows that the interpretation of OOA volatility derived from molecular composition is complex, and warrants careful consideration of various parameters (Graham et al., 2022;Voliotis et al., 2021).

340   The urban site in Delhi, India (UDL) exhibits the lowest LVOC and lowest ELVOC mass fractions (13.4% in total), highest IVOC mass fractions (54.5±3.4%) and mass-weighted $\log_{10}C_{sat}$ (T) values (2.3±0.3 µg m^{-3}; also consistent with its lowest O:C ratios, see Figure 1a), compared to the two urban sites in Germany (UKA: LVOC+ELVOC: 18.4–42.1%; IVOC: 20.5–42.8%; $\log_{10}C_{sat}$ (T): -0.37–1.6 µg m^{-3}; UST: LVOC+ELVOC: 27.9–

41.9%; IVOC: 23.8–32.5%; $\log_{10}C_{sat}$ (T): -0.50–0.63 µg m^{-3}). The relatively higher volatility of OOA in Delhi

345   compared to that in the German cities may be likely related to the dominance of primary OA with very high biomass burning (also reflected in the large peak of C$_6$ compounds in Figure S1) and traffic emissions (Kumar et al., 2022). The biomass burning vapors have been found to be responsible for the nighttime particle growth at UDL (Mishra et al., 2023). As for UKA and UST, higher LVOC and ELVOC mass fractions (41.9–42.1%) and lower mass-weighted $\log_{10}C_{sat}$ (T) values (-0.50–-0.37 µg m^{-3}) are observed in winter compared to summer (18.4–27.9%

350   and 0.63–1.6 µg m^{-3}, respectively), indicating that the bulk winter OOA is less volatile. Similar results were also observed in Zurich, Switzerland based on AMS data (Canonaco et al., 2015). Higher O:C ratios (Figure 1a) could be part of the reason for the less volatile OOA in winter in Stuttgart (UST) compared to summer (Huang et al., 2019b). For the Karlsruhe curb site (UKA), the O:C ratios are quite similar for winter and summer (Figure 1a) and therefore other factors, such as the relatively higher contributions of larger molecules (nC >16; Figure S1) as well

355   as the reduced volatility of OOA from biomass burning due to aging processes (Keller and Burtscher, 2017) (see also the higher O:C ratios in Figure 1a compared to UDL with more primary emissions (Kumar et al., 2022)), might play a role.
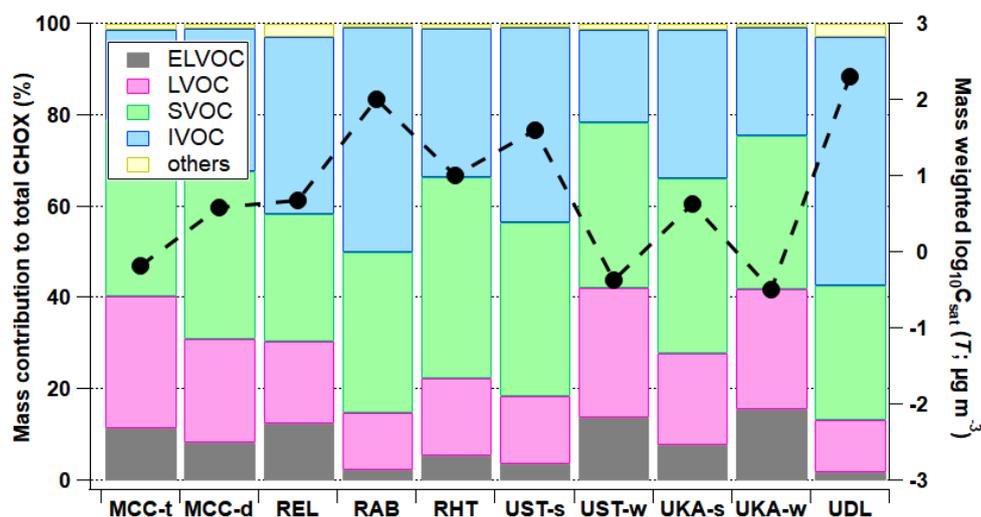
Figure 2. Campaign-average contribution (%) to total organics of different volatility groups resulting from VBS

360   calculations (colored in bars) and campaign-average mass-weighted $\log_{10}C_{sat}$ (T) values (in black markers) for different campaigns with the modified Li et al. (2016) parametrization method (Daumit et al., 2013; Isaacman-VanWertz and Aumont, 2021). Compounds more volatile than IVOC with C_{sat} (T) higher than $10^{6.5}$ µg m^{-3} (labelled as "others") contributed negligibly (0.8−2.9%).

The mass-weighted $\log_{10}C_{sat}$ (T) shows a qualitatively similar distribution as the ambient temperature

365   (Pearson's R: 0.58; Figure S3 and S4). This makes sense insofar as on the one hand the $\log_{10}C_{sat}$ (T) calculated using molecular composition is shifted based on ambient temperature (compare Eq. 2) - the same compound exhibits a higher apparent volatility under warmer conditions and vice versa; on the other hand, a higher apparent volatility is also expected at higher ambient temperatures due to higher local emissions of biogenic precursors. In addition, we find a positive correlation between $\log_{10}C_{sat}$ (T) and humidity (Pearson's R for RH and absolute

370   humidity: 0.57 and 0.68, respectively; Figure S4), indicating potential hydrolysis effects on OOA particles

(forming smaller and more volatile compounds) caused by potentially high aerosol liquid water content at higher humidity levels (Lee et al., 2020;Hu et al., 2011;Hinks et al., 2018). Negative correlations are found between $\log_{10}C_{sat}$ (*T*) vs. nO (Pearson's R: -0.72) and the average mass-weighted molecular weight (MW) of CHOX compounds (Pearson's R: -0.56), following the parametrization assumption of the oxidation effect on volatility

375 and of lower volatility for larger and complex molecules (Donahue et al., 2011).

3.2.2 Volatility derived from thermograms

We further investigate the volatility derived from FIGAERO thermograms qualitatively for the different sites and compare it to the volatility derived from the molecular composition measurements. It is important to note that, similar to D'Ambro et al. (2018), the term "volatility" we discuss here refers to the effective volatility of bulk

380 OOA particles, which combines the impacts of diffusion limitations and thermal decomposition of lower-volatility species. We focus the bulk OOA volatility analysis here on the shape and distribution of sum thermograms, which are found to give representative qualitative volatility estimations as they take into account the whole signal distribution and reduce potential artefacts from thermal decomposition of individual compounds (Voliotis et al., 2021).

385 Campaign-average sum thermograms of CHOX compounds for the different locations are shown in Figure 3, normalized to their maximum values. Thermogram shapes vary for different environments, and they exhibit maximum signal at temperatures (sumT$_{max}$) ranging from 80.5 to 146.3 °C (see also Figure S5). Such differences of sumT$_{max}$ of >60 °C across different systems and environments are hardly surprising, given the large spread in T$_{max}$ for all compounds in one single mass spectrum (Huang et al., 2019b;Wang and Ruiz, 2018), in T$_{max}$

390 calibrations with different instrumental settings, experimental procedures or calibrants (Wang et al., 2020;Ylisirniö et al., 2021), as well as for one compound with the same molecular formula between day vs. night (Thompson et al., 2017;Gaston et al., 2016), field vs. laboratory (Thompson et al., 2017), or over a whole campaign period (Thompson et al., 2017) (see an example of $C_6H_{10}O_5$, the molecular formula corresponding to levoglucosan, in Figure S6). It is also worth noting that thermal decomposition of larger organic compounds during particle

395 desorption with the FIGAERO could form products with lower masses and lower T$_{max}$ values, and hence higher effective volatility. Although the calculated decomposition fraction has a minor effect on the molecular composition of OOA particles (see more details in section 3.2.1), the contribution of fragments to their parent compounds and the impact on the "original" volatility should not be ignored.

The mountain site in Bolivia in the transition season (MCC-t) exhibits some of the lowest sumT$_{max}$ values of

400 all stations (81.7 °C), indicating relatively higher bulk volatility. In contrast, during the dry season, the bulk OOA appears less volatile (MCC-d sumT$_{max}$: 107.7 °C). This trend is in disagreement with $\log_{10}C_{sat}$ (*T*), which is higher for MCC-d (i.e. higher volatility) than MCC-t. The discrepancy could be due to thermal fragmentation of larger oligomeric molecules, which bias the C_{sat} results towards higher volatilities and the sum thermogram shape to a lesser extent due to the dominance of monomer species (i.e., ending up with a "tail"). Compared to MCC-t

405 (~26.6%), MCC-d exhibits a higher contribution of thermal fragmentation (~35.9%; also reflected in the higher IVOC fractions in Figure 2a), with multi-mode thermograms showing elevated signals at high desorption temperatures (~150 °C), i.e., with long "tails" (see also Figure S5a–b).

The rural sites in Germany (REL) and southeastern U.S. (RAB) have similar sumT$_{max}$ values of ~100°C. Both also show contributions (up to 21%) from thermal fragmentation through multi-mode thermograms or long tails at

410 high desorption temperatures (~150 °C; see also Figure S5c–d; similar to the dry season for the mountain site

MCC-d). The lowest sumT$_{max}$ value (94.5 °C) at RAB is consistent with its highest average $\log_{10}C_{sat}$ (T) value (2.0±0.4 µg m^{-3}) among the rural stations. The rural site in Finland (RHT) exhibits a high sumT$_{max}$ value of 146.3 °C with a thermogram shape reaching a plateau after 120 °C and the signal only starting to decrease at a desorption temperature >180 °C (see also Figure S5e). This might be related to an older age (D'Ambro et al., 2018) and/or a

415 more viscous phase state of the OOA particles at RHT caused by its lowest temperature and RH of all rural stations (Table S1) (Shiraiwa et al., 2011), affecting the evaporative behavior and inferred volatility of the particle-bound compounds (Yli-Juuti et al., 2017;Huang et al., 2018).

The urban sites in Germany (UKA and UST) exhibit similar trends in sumT$_{max}$, with relatively higher values in winter (106.1–112.5 °C) compared to summer (80.5–102.0 °C). Such a seasonal trend is mirrored in their

420 average $\log_{10}C_{sat}$ (T) values. Differences in sumT$_{max}$ between summer and winter are found to be larger for Stuttgart (UST; ~32 °C) than for Karlsruhe (UKA; ~4 °C). This could be due to the differences in measurement environments and topography. The topography at UST prevents dispersion (Huang et al., 2019b;Baumbach and Vogt, 2003), and thus the formation of more oxygenated molecules in winter at UST can be expected due to longer residence time of the air masses (Buchholz et al., 2019) (also reflected in the higher O:C ratios; see Figure 1a).

425 The UKA site is a curb site with more influence from direct traffic emissions (Kumar et al., 2022) including larger aromatic compounds (Lim et al., 1999;Zheng et al., 2017) (see above-mentioned discussions and Figure S1), and smaller differences for summer vs. winter are therefore expected. The winter Delhi site in India (UDL) exhibits a similar sumT$_{max}$ value (113.0 °C) as UST and UKA in winter (106.1–112.5 °C). All three urban locations show indication of substantial contribution (up to 14%) of thermal fragmentation in their thermograms (see also Figure

430 S5f–j), which might also be the reason for the highest sumT$_{max}$ value not corresponding to the lowest $\log_{10}C_{sat}$ (T) value, similar to MCC.

As shown in earlier publications (Huang et al., 2018;Ylisirniö et al., 2021), the connection between T$_{max}$ and volatility is complex, and direct relationships between T$_{max}$ and vapor pressures can only be established for solutions of pure or few compound(s) (Wang et al., 2020;Ylisirniö et al., 2021;Ren et al., 2022). For the complex

435 ambient particle matrix, other factors than the pure compounds' vapor pressures come into play, such as the presence of isomers with different vapor pressures (Thompson et al., 2017), thermal decomposition contributions of larger molecules (Lopez-Hilfiker et al., 2015), and matrix effects and viscosity (Huang et al., 2018;D'Ambro et al., 2017;Wang and Ruiz, 2018). This is exemplified here showing varying T$_{max}$ values for compounds with the same molecular formula across different campaigns (with an average T$_{max}$ difference of 55.0±24.3 °C), such as

440 $C_5H_{12}O_4$ (molecular formula corresponding to 2-methyltetrol, a tracer of isoprene oxidation products (D'Ambro et al., 2019)), $C_6H_{10}O_5$ (molecular formula corresponding to levoglucosan, a tracer for biomass burning (Saarnio et al., 2010)), $C_8H_{10}O_5$ (identified in the laboratory as a monoterpene oxidation product (Hammes et al., 2019)), $C_8H_{12}O_5$ (molecular formula corresponding to 2-hydroxyterpenylic acid identified in α-pinene SOA (Claeys et al., 2009)), $C_{10}H_{15}NO_7$ (identified in the laboratory as a monoterpene oxidation product (Boyd et al., 2015;Faxon et

445 al., 2018)), and $C_{17}H_{24}O_6$ (identified in the laboratory as a monoterpene oxidation product (Kenseth et al., 2020); Figure S7). Such variations may be due to actual changes in effective volatilities of the observed OOA components, due to experimental factors, or both. For example, correction of the T$_{max}$ values to a filter mass loading of 1 µg following our approach outlined earlier (Huang et al., 2018) only leads to a T$_{max}$ change of <5 °C, which is not enough to explain the T$_{max}$ differences alone. We conclude that the analysis and interpretation of OOA volatility

450 based on FIGAERO-CIMS thermograms is challenging and, in the absence of additional constraints on OOA

composition and thermal behavior, currently remains at the qualitative level (Graham et al., 2022;Voliotis et al., 2021), especially for complex field data.

Similar to $\log_{10}C_{sat}$ (T), we also compare the sumT$_{max}$ with various environmental and measurement parameters (Figure S8). Correlations of sumT$_{max}$ values with other parameters (e.g., meteorology, trace gases) are weak

455 (Pearson's R within ±0.3), except for SO$_2$ (Pearson's R: -0.67). However, this could be artificial as SO$_2$ would not react/condense directly onto aerosol particles and also too few SO$_2$ data points were available for this correlation. Levels of sulfur-containing organics (CHOS and CHONS) and non-refractory particulate sulfate show no correlations with sumT$_{max}$ values as well. These results further show the complexity in assessing the effective volatility derived from thermogram behavior and T$_{max}$, especially for a diverse set of field data. Contributing to the

460 lack of clear correlations in this analysis may be potential effects of experimental parameters on the FIGAERO thermograms (Table S2) (Thornton et al., 2020), as well as open questions in their interpretation, as noted above.
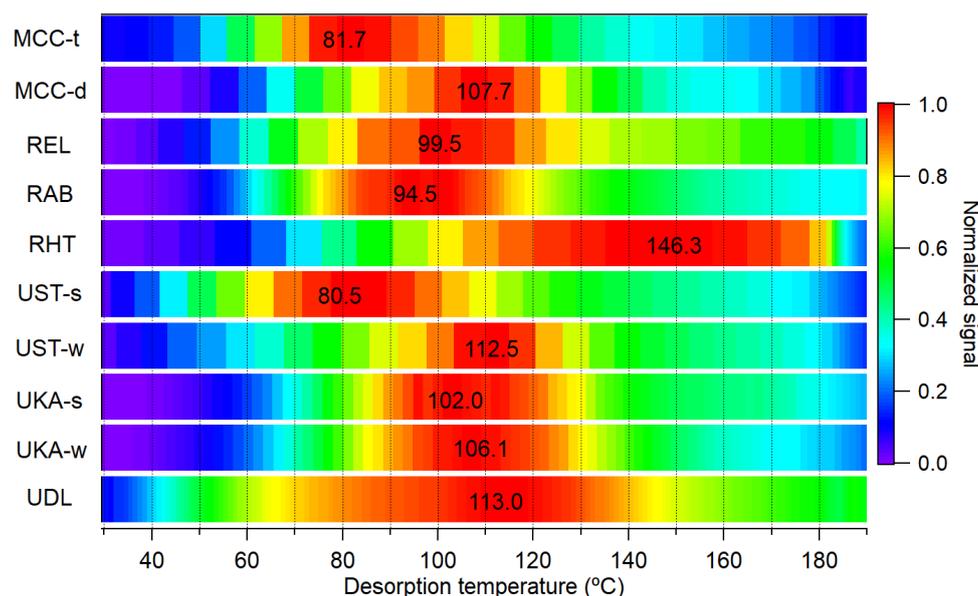

Figure 3. Campaign-average sum thermograms of CHOX compounds (normalized to their maximum values) for all campaigns with corresponding sumT$_{max}$ values labeled on the plot.

465 **3.3 Relationship between thermal desorption-derived volatility and molecular composition-derived volatility**

In order to investigate whether there is consistency in the bulk OOA volatility derived from molecular composition and thermograms, we compare the average $\log_{10}C_{sat}$ (i.e, molecular composition-derived volatility) with the sumT$_{max}$ (i.e., thermal desorption-derived volatility) in Figure 4 and Figure S9. The gray area covers the previously

470 reported calibration fit curves of $\log_{10}C_{sat}$ (298 K) vs. calibrant T$_{max}$ values in colored dashed lines. As we can see from Figure 4, overall the $\log_{10}C_{sat}$ (298 K) values from different locations are close to the range given by the calibration curves. However, it is important to note that this does not suggest T$_{max}$ calibrations are not needed for field measurements (unavailable for our datasets). Although we cannot find a correlation between $\log_{10}C_{sat}$ (298 K) and sumT$_{max}$ with all data points included, that correlation might be to some extent improved with laboratory

475   T_{max} calibrations. This underlines again the complexity of assessments of the volatility through either method, as already shown for laboratory measurements (Graham et al., 2022), but even more so for comparisons of complex ambient data from different locations and periods, and different instrument versions (see Table S2).

If we only focus on the datasets collected with the same FIGAERO setup (REL, UST-s, UST-w, UKA-s, and UKA-w) assuming similar calibration factors, a negative correlation (Pearson's R: -0.54) is observed between

480    $\log_{10}C_{sat}$ (298 K) and $sumT_{max}$. And the correlation still holds between ambient temperature-corrected $\log_{10}C_{sat}$ and $sumT_{max}$ (Pearson's R: -0.92). Although C_{sat} values can be biased by orders of magnitude using other parametrization methods (Graham et al., 2022), the general slope and trend is similar to the calibration curves. The results hence provide an overall broad qualitative agreement between bulk volatility derived from thermograms and composition.
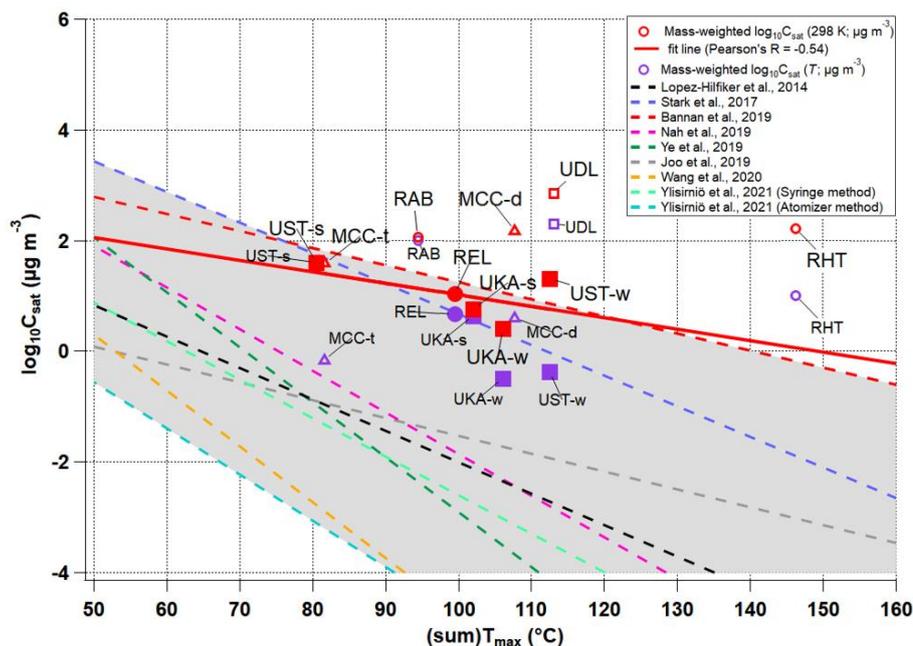
485

Figure 4. Comparison of the campaign-average mass-weighted $\log_{10}C_{sat}$ and $sumT_{max}$ values for different locations and seasons (Mountain sites in triangles, Rural sites in circles, and Urban sites in squares), with mass-weighted $\log_{10}C_{sat}$ (298 K) in red and mass-weighted $\log_{10}C_{sat}$ (T) in purple. The red solid line is the fit line for the red solid markers only, the data of which are from the same FIGEARO setup. The gray area covers the previously reported

490   calibrations of $\log_{10}C_{sat}$ (298 K) vs. calibrant T_{max} values in colored dashed lines. The wide spread of these calibration lines is believed to result from variations in instrument designs, experimental procedures, and the ranges of used calibration compounds (Ylisirniö et al., 2021).

Other than the effects of different FIGAERO geometries (Ylisirniö et al., 2021), parameters affecting the correlation between $\log_{10}C_{sat}$ and $sumT_{max}$ are manifold and the correlation is subject to uncertainties and artefacts

495   for both methods. On the one hand, molecular composition-derived volatility is limited by its incapability in differentiating isomers with different vapor pressures since it is solely based on molecular formula (Graham et al., 2022), and the bulk OOA volatility may also diverge from the sum of individual parametrized C_{sat} due to non-ideal

intermolecular interactions (Compernolle et al., 2011;Isaacman-VanWertz and Aumont, 2021). On the other hand, thermal desorption-derived volatility can suffer from artefacts from oligomer content, viscosity, and possible

500   mutual interactions between them (i.e., oligomer content vs. viscosity) (Huang et al., 2018;D'Ambro et al., 2017;Wang and Ruiz, 2018). Thermal decomposition of larger oligomeric molecules can bias the C_{sat} towards higher volatilities and the sum thermogram shape and sumT$_{max}$ to a lesser extent due to the dominance of monomer species (i.e., ending up with a longer tail). There have been attempts to separate the thermal decomposition contribution for individual thermograms (Lutz et al., 2019;D'Ambro et al., 2018;Buchholz et al., 2020), but this

505   poses the threat for introducing new uncertainties due to the difficulty in e.g. differentiating isomers from thermal decomposition products, and monomers from dimers in ambient samples with complex VOC precursors (Graham et al., 2022;Voliotis et al., 2021). Overall, however, for a limited number of our datasets from the exact same instrument, the lower apparent volatility (i.e., higher sumT$_{max}$) agree qualitatively with the lower $\log_{10}C_{sat}$ values, corroborating potential relationships between volatility and chemical composition across different environments

510   and systems.

4 Conclusions and atmospheric implications

In this paper, the molecular composition and volatility of OOA particles at different rural, urban, and remote environments across the globe were investigated with the deployments of FIGAERO-CIMS. We find distinct molecular composition for different environments: OOA particles exhibit on average larger nC and lower O:C

515   ratios at the urban sites (nC: 9.8±0.7; O:C: 0.76±0.03), followed by the rural (nC: 8.8±0.6; O:C: 0.80±0.05) and remote mountain stations (nC: 8.1±0.8; O:C: 0.91±0.07), indicative of different emission sources and chemistry. While the CHO contributions are on average higher (79.9±5.2%) compared to the mountain (66.2±5.5%) and urban sites (72.6±4.3%), in accordance with their proximity to forested areas, the largest contributions of CHON compounds are found at the urban stations (27.1±4.3%), consistent with their higher NO$_x$ levels.

520   Besides, the bulk OOA volatility differences are found in C_{sat} values by up to ~3 orders of magnitude, and in thermogram shapes with average sumT$_{max}$ values by up to 60 °C across different locations and systems. Despite of the uncertainties/limitations for volatility derived from both sumT$_{max}$ and molecular formula as well as the translated uncertainties in the relationship between them, sumT$_{max}$ are found to exhibit an overall negative correlation with molecular formula based C_{sat}, suggesting a potential relationship between the volatility and

525   chemical composition for the different locations and systems.

Here, using FIGAERO-CIMS measurements of OOA particles from various locations across the globe, we achieve a comprehensive picture of the relationship between volatility and chemical composition of OOA particles in different rural, urban, and remote environments, which are characterized by different ambient meteorological parameters, trace gas levels, emission sources/chemistry, and resulting distinct OOA molecular composition and

530   volatility. Our study shows a connection between chemical composition and thermal desorption behavior, but also the limitations of using measurements of either for the assessment of volatility. Thermal decomposition has been a well-known issue for FIGAERO-CIMS measurements, however, the effects on the bulk molecular composition and sum thermograms of all detected OOA compounds are small as these thermally-unstable oligomers do not dominate the OOA mass. Still, alternative approaches need to be developed for more quantitative estimations of

535   volatility from FIGAERO-CIMS measurements.

Overall we find that it is clearly the chemical composition of OOA that determines its apparent volatility, and that environmental conditions (e.g., ambient temperature) play a lesser, secondary role through their influence on sources and chemistry of a particular environment, such as seasonal patterns of biogenic emissions and human behavior (e.g., residential heating). For example, summer OOA particles tend to be more volatile than the winter

540   OOA particles due to higher ambient temperatures in summer and consequently higher local emissions of biogenic precursors and higher reaction rates. In winter, OOA particles are subject to higher biomass burning emissions and/or traffic emissions from human activities. Therefore, the importance of chemical composition and environmental conditions (e.g., ambient temperature) on the apparent volatility of OOA particles is different, with the chemical composition (i.e., sources and chemistry) being a more direct and important factor than the

545   environmental conditions. The comprehensive global dataset from our results shows the complex thermodynamics and chemistry of OOA and their changes during its lifetime in the atmosphere, and that the chemical description of OOA generally suffices to predict its apparent volatility, at least qualitatively. Our study thus provides new insights that will help guide choices of e.g. descriptions of OOA volatility in different model frameworks, which has been previously simplified due to challenges to measure and represent it in models. A better understanding of

550   the chemical nature and volatility of OA components can thus ultimately improve predictions of atmospheric organic particle mass and climate effects of atmospheric OA.

Data availability

The data that are involved in the figures can be found at https://doi.org/10.5281/zenodo.7983797 (Huang, 2023).

Author contributions

555   JT, HS, DG, and CM designed the research; WH, CW, LG, YG, SLH, FDL, BHL, JS, XS, RR, SNT, DG, FJ, MV, and CM conducted field measurements; WH, CW, LG, SLH, FDL, BHL, JS, HS, XS, SNT, DG, and CM analysed the data; CW, LG, YG, SLH, JT, SS, TY, JS, HS, XS, MV, and CM provided suggestions for the data analysis, interpretation, and discussion; WH and CM wrote the paper with contributions of all authors. All authors have given approval to the final text.

560   **Competing interests**

At least one of the (co-)authors is a member of the editorial board of Atmospheric Chemistry and Physics.

References

Aliaga, D., Sinclair, V. A., Andrade, M., Artaxo, P., Carbone, S., Kadantsev, E., Laj, P., Wiedensohler, A., Krejci, R., and Bianchi, F.: Identifying source regions of air masses sampled at the tropical high-altitude site of Chacaltaya using WRF-FLEXPART and cluster analysis, Atmos Chem Phys, 21, 16453-16477, https://doi.org/10.5194/acp-
585 21-16453-2021, 2021.

Bardakov, R., Thornton, J. A., Riipinen, I., Krejci, R., and Ekman, A. M. L.: Transport and chemistry of isoprene and its oxidation products in deep convective clouds, Tellus B, 73, 1979856, https://doi.org/10.1080/16000889.2021.1979856, 2021.

Baumbach, G., and Vogt, U.: Influence of inversion layers on the distribution of air pollutants in urban areas, Water,
590 Air, & Soil Pollution: Focus, 3, 67–78, https://doi.org/10.1023/A:1026098305581, 2003.

Bianchi, F., Sinclair, V. A., Aliaga, D., Zha, Q., Scholz, W., Wu, C., Heikkinen, L., Modini, R., Partoll, E., Velarde, F., Moreno, I., Gramlich, Y., Huang, W., Leiminger, M., Enroth, J., Peräkylä, O., Marinoni, A., Xuemeng, C., Blacutt, L., Forno, R., Gutierrez, R., Ginot, P., Uzu, G., Facchini, M. C., Gilardoni, S., Gysel-Beer, M., Cai, R., Petäjä, T., Rinaldi, M., Saathoff, H., Sellegri, K., Worsnop, D., Artaxo, P., Hansel, A., Kulmala, M., Wiedensohler,
595 A., Laj, P., Krejci, R., Carbone, S., Andrade, M., and Mohr, C.: The SALTENA Experiment: Comprehensive Observations of Aerosol Sources, Formation, and Processes in the South American Andes, Bulletin of the American Meteorological Society, E212–E229, https://doi.org/10.1175/BAMS-D-20-0187.1, 2022.

Boyd, C. M., Sanchez, J., Xu, L., Eugene, A. J., Nah, T., Tuet, W. Y., Guzman, M. I., and Ng, N. L.: Secondary organic aerosol formation from the beta-pinene+NO3 system: effect of humidity and peroxy radical fate, Atmos
600 Chem Phys, 15, 7497–7522, https://doi.org/10.5194/acp-15-7497-2015, 2015.

Buchholz, A., Lambe, A. T., Ylisirniö, A., Li, Z., Tikkanen, O.-P., Faiola, C., Kari, E., Hao, L. Q., Luoma, O., Huang, W., Mohr, C., Worsnop, D. R., Nizkorodov, S. A., Yli-Juuti, T., Schobesberger, S., and Virtanen, A.: Insights into the O:C-dependent mechanisms controlling the evaporation of α-pinene secondary organic aerosol particles, Atmos Chem Phys, 19, 4061–4073, https://doi.org/10.5194/acp-19-4061-2019, 2019.

605　Buchholz, A., Ylisirnio, A., Huang, W., Mohr, C., Canagaratna, M., Worsnop, D., Schobesberger, S., and Virtanen, A.: Deconvolution of FIGAERO-CIMS thermal desorption profiles using positive matrix factorisation to identify chemical and physical processes during particle evaporation, Atmos Chem Phys, 20, 7693-7716, https://doi.org/10.5194/acp-20-7693-2020, 2020.

　　　Cai, J., Daellenbach, K. R., Wu, C., Zheng, Y., Zheng, F. X., Du, W., Haslett, S. L., Chen, Q., Kulmala, M., and
610　Mohr, C.: Characterization of offline analysis of particulate matter with FIGAERO-CIMS, Atmos Meas Tech, 16, 1147-1165, https://doi.org/10.5194/amt-16-1147-2023, 2023.

　　　Canonaco, F., Slowik, J. G., Baltensperger, U., and Prévôt, A. S. H.: Seasonal differences in oxygenated organic aerosol composition: implications for emissions sources and factor analysis, Atmos Chem Phys, 15, 6993–7002, https://doi.org/10.5194/acp-15-6993-2015, 2015.

615　Claeys, M., Iinuma, Y., Szmigielski, R., Surratt, J. D., Blockhuys, F., Van Alsenoy, C., Böge, O., Sierau, B., Gómez-González, Y., Vermeylen, R., Van der Veken, P., Shahgholi, M., Chan, A. W. H., Herrmann, H., Seinfeld, J. H., and Maenhaut, W.: Terpenylic acid and related compounds from the oxidation of α-pinene: Implications for new particle formation and growth above forests, Environ Sci Technol, 43, 6976–6982, https://doi.org/10.1021/es9007596, 2009.

620　Compernolle, S., Ceulemans, K., and Muller, J. F.: EVAPORATION: a new vapour pressure estimation methodfor organic molecules including non-additivity and intramolecular interactions, Atmos Chem Phys, 11, 9431-9450, https://doi.org/10.5194/acp-11-9431-2011, 2011.

　　　D'Ambro, E. L., Lee, B. H., Liu, J. M., Shilling, J. E., Gaston, C. J., Lopez-Hilfiker, F. D., Schobesberger, S., Zaveri, R. A., Mohr, C., Lutz, A., Zhang, Z. F., Gold, A., Surratt, J. D., Rivera-Rios, J. C., Keutsch, F. N., and Thornton,
625　J. A.: Molecular composition and volatility of isoprene photochemical oxidation secondary organic aerosol under low- and high-NOx conditions, Atmos Chem Phys, 17, 159–174, https://doi.org/10.5194/acp-17-159-2017, 2017.

　　　D'Ambro, E. L., Schobesberger, S., Zaveri, R. A., Shilling, J. E., Lee, B. H., Lopez-Hilfiker, F. D., Mohr, C., and Thornton, J. A.: Isothermal Evaporation of alpha-Pinene Ozonolysis SOA: Volatility, Phase State, and Oligomeric Composition, Acs Earth Space Chem, 2, 1058-1067, https://doi.org/10.1021/acsearthspacechem.8b00084, 2018.

630　D'Ambro, E. L., Schobesberger, S., Gaston, C. J., Lopez-Hilfiker, F. D., Lee, B. H., Liu, J., Zelenyuk, A., Bell, D., Cappa, C. D., Helgestad, T., Li, Z., Guenther, A., Wang, J., Wise, M., Caylor, R., Surratt, J. D., Riedel, T., Hyttinen, N., Salo, V.-T., Hasan, G., Kurtén, T., Shilling, J. E., and Thornton, J. A.: Chamber-based insights into the factors controlling epoxydiol (IEPOX) secondary organic aerosol (SOA) yield, composition, and volatility, Atmos Chem Phys, 19, 11253–11265, https://doi.org/10.5194/acp-19-11253-2019, 2019.

635　Daumit, K. E., Kessler, S. H., and Kroll, J. H.: Average chemical properties and potential formation pathways of highly oxidized organic aerosol, Faraday Discuss, 165, 181-202, https://doi.org/10.1039/C3FD00045A, 2013.

　　　Donahue, N. M., Robinson, A. L., and Pandis, S. N.: Atmospheric organic particulate matter: from smoke to secondary organic aerosol, Atmos Environ, 43, 94–106, https://doi.org/10.1016/j.atmosenv.2008.09.055, 2009.

　　　Donahue, N. M., Epstein, S. A., Pandis, S. N., and Robinson, A. L.: A two-dimensional volatility basis set: 1.
640　organic-aerosol mixing thermodynamics, Atmos Chem Phys, 11, 3303–3318, https://doi.org/10.5194/acp-11-3303-2011, 2011.

　　　Donahue, N. M., Kroll, J. H., Pandis, S. N., and Robinson, A. L.: A two-dimensional volatility basis set – Part 2: diagnostics of organic-aerosol evolution, Atmos Chem Phys, 12, 615–634, https://doi.org/10.5194/acp-12-615-2012, 2012.

645 Epstein, S. A., Riipinen, I., and Donahue, N. M.: A semiempirical correlation between enthalpy of vaporization and saturation concentration for organic aerosol, Environ Sci Technol, 44, 743–748, https://doi.org/10.1021/es902497z, 2010.

Faxon, C., Hammes, J., Le Breton, M., Pathak, R. K., and Hallquist, M.: Characterization of organic nitrate constituents of secondary organic aerosol (SOA) from nitrate-radical-initiated oxidation of limonene using high-

650 resolution chemical ionization mass spectrometry, Atmos Chem Phys, 18, 5467–5481, https://doi.org/10.5194/acp-18-5467-2018, 2018.

Fry, J. L., Brown, S. S., Middlebrook, A. M., Edwards, P. M., Campuzano-Jost, P., Day, D. A., Jimenez, J. L., Allen, H. M., Ryerson, T. B., Pollack, I., Graus, M., Warneke, C., de Gouw, J. A., Brock, C. A., Gilman, J., Lerner, B. M., Dube, W. P., Liao, J., and Welti, A.: Secondary organic aerosol (SOA) yields from NO3 radical + isoprene

655 based on nighttime aircraft power plant plume transects, Atmos Chem Phys, 18, 11663-11682, https://doi.org/10.5194/acp-18-11663-2018, 2018.

Gaston, C. J., Lopez-Hilfiker, F. D., Whybrew, L. E., Hadley, O., McNair, F., Gao, H. L., Jaffe, D. A., and Thornton, J. A.: Online molecular characterization of fine particulate matter in Port Angeles, WA: Evidence for a major impact from residential wood smoke, Atmos Environ, 138, 99–107,

660 https://doi.org/10.1016/j.atmosenv.2016.05.013, 2016.

Graham, E. L., Wu, C., Bell, D. M., Bertrand, A., Haslett, S. L., Baltensperger, U., El Haddad, I., Krejci, R., Riipinen, I., and Mohr, C.: Volatility of aerosol particles from NO3 oxidation of various biogenic organic precursors, EGUsphere, [preprint], https://doi.org/10.5194/egusphere-2022-1043, 2022.

Hallquist, M., Wenger, J. C., Baltensperger, U., Rudich, Y., Simpson, D., Claeys, M., Dommen, J., Donahue, N. M.,

665 George, C., Goldstein, A. H., Hamilton, J. F., Herrmann, H., Hoffmann, T., Iinuma, Y., Jang, M., Jenkin, M. E., Jimenez, J. L., Kiendler-Scharr, A., Maenhaut, W., McFiggans, G., Mentel, T. F., Monod, A., Prévôt, A. S. H., Seinfeld, J. H., Surratt, J. D., Szmigielski, R., and Wildt, J.: The formation, properties and impact of secondary organic aerosol: current and emerging issues, Atmos Chem Phys, 9, 5155–5236, https://doi.org/10.5194/acp-9-5155-2009, 2009.

670 Hammes, J., Lutz, A., Mentel, T., Faxon, C., and Hallquist, M.: Carboxylic acids from limonene oxidation by ozone and hydroxyl radicals: insights into mechanisms derived using a FIGAERO-CIMS, Atmos Chem Phys, 19, 13037–13052, https://doi.org/10.5194/acp-19-13037-2019, 2019.

Hinks, M. L., Montoya-Aguilera, J., Ellison, L., Lin, P., Laskin, A., Laskin, J., Shiraiwa, M., Dabdub, D., and Nizkorodov, S. A.: Effect of relative humidity on the composition of secondary organic aerosol from the oxidation

675 of toluene, Atmos Chem Phys, 18, 1643-1652, https://doi.org/10.5194/acp-18-1643-2018, 2018.

Hu, K. S., Darer, A. I., and Elrod, M. J.: Thermodynamics and kinetics of the hydrolysis of atmospherically relevant organonitrates and organosulfates, Atmos Chem Phys, 11, 8307–8320, https://doi.org/10.5194/acp-11-8307-2011, 2011.

Huang, W.: Figure data of "Variation in chemical composition and volatility of oxygenated organic aerosol in

680 different rural, urban, and remote environments", Zenodo [data set], https://doi.org/10.5281/zenodo.7983797, 2023.

Huang, W., Saathoff, H., Pajunoja, A., Shen, X. L., Naumann, K.-H., Wagner, R., Virtanen, A., Leisner, T., and Mohr, C.: α-Pinene secondary organic aerosol at low temperature: chemical composition and implications for particle viscosity, Atmos Chem Phys, 18, 2883–2898, https://doi.org/10.5194/acp-18-2883-2018, 2018.

685   Huang, W., Saathoff, H., Shen, X., Ramisetty, R., Leisner, T., and Mohr, C.: Chemical characterization of highly functionalized organonitrates contributing to night-time organic aerosol mass loadings and particle growth, Environ Sci Technol, 53, 1165–1174, https://doi.org/10.1021/acs.est.8b05826, 2019a.

Huang, W., Saathoff, H., Shen, X. L., Ramisetty, R., Leisner, T., and Mohr, C.: Seasonal characteristics of organic aerosol chemical composition and volatility in Stuttgart, Germany, Atmos Chem Phys, 19, 11687–11700, https://doi.org/10.5194/acp-19-11687-2019, 2019b.

690   Huang, W., Li, H. Y., Sarnela, N., Heikkinen, L., Tham, Y. J., Mikkila, J., Thomas, S. J., Donahue, N. M., Kulmala, M., and Bianchi, F.: Measurement report: Molecular composition and volatility of gaseous organic compounds in a boreal forest - from volatile organic compounds to highly oxygenated organic molecules, Atmos Chem Phys, 21, 8961–8977, https://doi.org/10.5194/acp-21-8961-2021, 2021.

Isaacman-VanWertz, G., and Aumont, B.: Impact of organic molecular structure on the estimation of
695   atmospherically relevant physicochemical parameters, Atmos Chem Phys, 21, 6541–6563, https://doi.org/10.5194/acp-21-6541-2021, 2021.

Jimenez, J. L., Canagaratna, M. R., Donahue, N. M., Prevot, A. S. H., Zhang, Q., Kroll, J. H., DeCarlo, P. F., Allan, J. D., Coe, H., Ng, N. L., Aiken, A. C., Docherty, K. S., Ulbrich, I. M., Grieshop, A. P., Robinson, A. L., Duplissy, J., Smith, J. D., Wilson, K. R., Lanz, V. A., Hueglin, C., Sun, Y. L., Tian, J., Laaksonen, A., Raatikainen, T.,
700   Rautiainen, J., Vaattovaara, P., Ehn, M., Kulmala, M., Tomlinson, J. M., Collins, D. R., Cubison, M. J., Dunlea, E. J., Huffman, J. A., Onasch, T. B., Alfarra, M. R., Williams, P. I., Bower, K., Kondo, Y., Schneider, J., Drewnick, F., Borrmann, S., Weimer, S., Demerjian, K., Salcedo, D., Cottrell, L., Griffin, R., Takami, A., Miyoshi, T., Hatakeyama, S., Shimono, A., Sun, J. Y., Zhang, Y. M., Dzepina, K., Kimmel, J. R., Sueper, D., Jayne, J. T., Herndon, S. C., Trimborn, A. M., Williams, L. R., Wood, E. C., Middlebrook, A. M., Kolb, C. E., Baltensperger,
705   U., and Worsnop, D. R.: Evolution of organic aerosols in the atmosphere, Science, 326, 1525–1529, https://doi.org/10.1126/science.1180353 2009.

Junninen, H., Ehn, M., Petäjä, T., Luosujärvi, L., Kotiaho, T., Kostiainen, R., Rohner, U., Gonin, M., Fuhrer, K., Kulmala, M., and Worsnop, D. R.: A high-resolution mass spectrometer to measure atmospheric ion composition, Atmos Meas Tech, 3, 1039–1053, https://doi.org/10.5194/amt-3-1039-2010, 2010.

710   Keller, A., and Burtscher, H.: Characterizing particulate emissions from wood burning appliances including secondary organic aerosol formation potential, J Aerosol Sci, 114, 21–30, https://doi.org/10.1016/j.jaerosci.2017.08.014, 2017.

Kenseth, C. M., Hafeman, N. J., Huang, Y., Dalleska, N. F., Stoltz, B. M., and Seinfeld, J. H.: Synthesis of Carboxylic Acid and Dimer Ester Surrogates to Constrain the Abundance and Distribution of Molecular Products
715   in alpha-Pinene and beta-Pinene Secondary Organic Aerosol, Environ Sci Technol, 54, 12829-12839, https://doi.org/10.1021/acs.est.0c01566, 2020.

Kiendler-Scharr, A., Mensah, A. A., Friese, E., Topping, D., Nemitz, E., Prevot, A. S. H., Äijälä, M., Allan, J., Canonaco, F., Canagaratna, M., Carbone, S., Crippa, M., Dall Osto, M., Day, D. A., De Carlo, P., Di Marco, C. F., Elbern, H., Eriksson, A., Freney, E., Hao, L., Herrmann, H., Hildebrandt, L., Hillamo, R., Jimenez, J. L.,
720   Laaksonen, A., McFiggans, G., Mohr, C., O'Dowd, C., Otjes, R., Ovadnevaite, J., Pandis, S. N., Poulain, L., Schlag, P., Sellegri, K., Swietlicki, E., Tiitta, P., Vermeulen, A., Wahner, A., Worsnop, D., and Wu, H.-C.: Ubiquity of organic nitrates from nighttime chemistry in the European submicron aerosol, Geophys Res Lett, 43, 7735–7744, https://doi.org/10.1002/2016GL069239, 2016.

Kroll, J. H., and Seinfeld, J. H.: Chemistry of secondary organic aerosol: Formation and evolution of low-volatility

725   organics in the atmosphere, Atmos Environ, 42, 3593–3624, https://doi.org/10.1016/j.atmosenv.2008.01.003, 2008.

Kumar, V., Giannoukos, S., Haslett, S. L., Tong, Y. D., Singh, A., Bertrand, A., Lee, C. P., Wang, D. S., Bhattu, D., Stefenelli, G., Dave, J. S., Puthussery, J. V., Qi, L., Vats, P., Rai, P., Casotto, R., Satish, R., Mishra, S., Pospisilova, V., Mohr, C., Bell, D. M., Ganguly, D., Verma, V., Rastogi, N., Baltensperger, U., Tripathi, S. N., Prévôt, A. S. H., and Slowik, J. G.: Highly time-resolved chemical speciation and source apportionment of organic aerosol

730   components in Delhi, India, using extractive electrospray ionization mass spectrometry, Atmos Chem Phys, 22, 7739-7761, https://doi.org/10.5194/acp-22-7739-2022, 2022.

Lee, B. H., Lopez-Hilfiker, F. D., Mohr, C., Kurtén, T., Worsnop, D. R., and Thornton, J. A.: An iodide-adduct high-resolution time-of-flight chemical-ionization mass spectrometer: Application to atmospheric inorganic and organic compounds, Environ Sci Technol, 48, 6309−6317, https://doi.org/10.1021/es500362a, 2014.

735   Lee, B. H., Mohr, C., Lopez-Hilfiker, F. D., Lutz, A., Hallquist, M., Lee, L., Romer, P., Cohen, R. C., Iyer, S., Kurtén, T., Hu, W. W., Day, D. A., Campuzano-Jost, P., Jimenez, J. L., Xu, L., Ng, N. L., Guo, H. Y., Weber, R. J., Wild, R. J., Brown, S. S., Koss, A., de Gouw, J., Olson, K., Goldstein, A. H., Seco, R., Kim, S., McAvey, K., Shepson, P. B., Starn, T., Baumann, K., Edgerton, E. S., Liu, J. M., Shilling, J. E., Miller, D. O., Brune, W., Schobesberger, S., D'Ambro, E. L., and Thornton, J. A.: Highly functionalized organic nitrates in the southeast

740   United States: Contribution to secondary organic aerosol and reactive nitrogen budgets, P Natl Acad Sci USA, 113, 1516–1521, https://doi.org/10.1073/pnas.1508108113, 2016.

Lee, B. H., Lopez-Hilfiker, F. D., D'Ambro, E. L., Zhou, P. T., Boy, M., Petäjä, T., Hao, L. Q., Virtanen, A., and Thornton, J. A.: Semi-volatile and highly oxygenated gaseous and particulate organic compounds observed above a boreal forest canopy, Atmos Chem Phys, 18, 11547–11562, https://doi.org/10.5194/acp-18-11547-2018, 2018.

745   Lee, B. H., D'Ambro, E. L., Lopez-Hilfiker, F. D., Schobesberger, S., Mohr, C., Zawadowicz, M. A., Liu, J., Shilling, J. E., Hu, W., Palm, B. B., Jimenez, J. L., Hao, L., Virtanen, A., Zhang, H., Goldstein, A. H., Pye, H. O. T., and Thornton, J. A.: Resolving ambient organic aerosol formation and aging pathways with simultaneous molecular composition and volatility observations, Acs Earth Space Chem, 4, 391-402, https://doi.org/10.1021/acsearthspacechem.9b00302, 2020.

750   Li, H. Y., Riva, M., Rantala, P., Heikkinen, L., Daellenbach, K., Krechmer, J. E., Flaud, P. M., Worsnop, D., Kulmala, M., Villenave, E., Perraudin, E., Ehn, M., and Bianchi, F.: Terpenes and their oxidation products in the French Landes forest: insights from Vocus PTR-TOF measurements, Atmos Chem Phys, 20, 1941–1959, https://doi.org/10.5194/acp-20-1941-2020, 2020.

Li, Y., Pöschl, U., and Shiraiwa, M.: Molecular corridors and parameterizations of volatility in the chemical

755   evolution of organic aerosols, Atmos Chem Phys, 16, 3327–3344, https://doi.org/10.5194/acp-16-3327-2016, 2016.

Lim, L. H., Harrison, R. M., and Harrad, S.: The Contribution of Traffic to Atmospheric Concentrations of Polycyclic Aromatic Hydrocarbons, Environ Sci Technol, 33, 3538–3542, https://doi.org/10.1021/es990392d, 1999.

Lopez-Hilfiker, F. D., Mohr, C., Ehn, M., Rubach, F., Kleist, E., Wildt, J., Mentel, T. F., Lutz, A., Hallquist, M., Worsnop, D., and Thornton, J. A.: A novel method for online analysis of gas and particle composition: description

760   and evaluation of a Filter Inlet for Gases and AEROsols (FIGAERO), Atmos Meas Tech, 7, 983−1001, https://doi.org/10.5194/amt-7-983-2014, 2014.

Lopez-Hilfiker, F. D., Mohr, C., Ehn, M., Rubach, F., Kleist, E., Wildt, J., Mentel, T. F., Carrasquillo, A. J., Daumit, K. E., Hunter, J. F., Kroll, J. H., Worsnop, D. R., and Thornton, J. A.: Phase partitioning and volatility of secondary organic aerosol components formed from α-pinene ozonolysis and OH oxidation: the importance of accretion

765   products and other low volatility compounds, Atmos Chem Phys, 15, 7765−7776, https://doi.org/10.5194/acp-15-7765-2015, 2015.

Lopez-Hilfiker, F. D., Mohr, C., D'Ambro, E. L., Lutz, A., Riedel, T. P., Gaston, C. J., Iyer, S., Zhang, Z., Gold, A., Surratt, J. D., Lee, B. H., Kurten, T., Hu, W. W., Jimenez, J., Hallquist, M., and Thornton, J. A.: Molecular composition and volatility of organic aerosol in the Southeastern U.S.: Implications for IEPOX derived SOA,

770   Environ Sci Technol, 50, 2200–2209, https://doi.org/10.1021/acs.est.5b04769, 2016.

Lutz, A., Mohr, C., Le Breton, M., Lopez-Hilfiker, F. D., Priestley, M., Thornton, J. A., and Hallquist, M.: Gas to Particle Partitioning of Organic Acids in the Boreal Atmosphere, Acs Earth Space Chem, 3, 1279-1287, https://doi.org/10.1021/acsearthspacechem.9b00041, 2019.

Masoud, C. G., and Ruiz, L. H.: Chlorine-Initiated Oxidation of α-Pinene: Formation of Secondary Organic Aerosol

775   and   Highly   Oxygenated   Organic   Molecules,   Acs   Earth   Space   Chem,   5,   2307–2319, https://doi.org/10.1021/acsearthspacechem.1c00150, 2021.

Mishra, S., Tripathi, S. N., Kanawade, V. P., Haslett, S. L., Dada, L., Ciarelli, G., Kumar, V., Singh, A., Bhattu, D., Rastogi, N., Daellenbach, K. R., Ganguly, D., Gargava, P., Slowik, J. G., Kulmala, M., Mohr, C., El-Haddad, I., and Prevot, A. S. H.: Rapid night-time nanoparticle growth in Delhi driven by biomass-burning emissions, Nat

780   Geosci, 16, 224-+, https://doi.org/10.1038/s41561-023-01138-x, 2023.

Mohr, C., Lopez-Hilfiker, F. D., Yli-Juuti, T., Heitto, A., Lutz, A., Hallquist, M., D'Ambro, E. L., Rissanen, M. P., Hao, L. Q., Schobesberger, S., Kulmala, M., Mauldin III, R. L., Makkonen, U., Sipilä, M., Petäjä, T., and Thornton, J. A.: Ambient observations of dimers from terpene oxidation in the gas phase: Implications for new particle formation and growth, Geophys Res Lett, 44, 2958−2966, https://doi.org/10.1002/2017gl072718, 2017.

785   Mohr, C., Thornton, J. A., Heitto, A., Lopez-Hilfiker, F. D., Lutz, A., Riipinen, I., Hong, J., Donahue, N. M., Hallquist, M., Petaja, T., Kulmala, M., and Yli-Juuti, T.: Molecular identification of organic vapors driving atmospheric nanoparticle growth, Nat Commun, 10, 4442, https://doi.org/10.1038/s41467-019-12473-2, 2019.

Murray, L. T.: Lightning NOx and Impacts on Air Quality, Curr Pollut Rep, 2, 115–133, https://doi.org/10.1007/s40726-016-0038-0, 2016.

790   Ng, N. L., Chhabra, P. S., Chan, A. W. H., Surratt, J. D., Kroll, J. H., Kwan, A. J., McCabe, D. C., Wennberg, P. O., Sorooshian, A., Murphy, S. M., Dalleska, N. F., Flagan, R. C., and Seinfeld, J. H.: Effect of NOx level on secondary organic aerosol (SOA) formation from the photooxidation of terpenes, Atmos Chem Phys, 7, 5159–5174, https://doi.org/10.5194/acp-7-5159-2007, 2007.

Nozière, B., Kaberer, M., Claeys, M., Allan, J., D'Anna, B., Decesari, S., Finessi, E., Glasius, M., Grgić, I., Hamilton,

795   J. F., Hoffmann, T., Iinuma, Y., Jaoui, M., Kahno, A., Kampf, C. J., Kourtchev, I., Maenhaut, W., Marsden, N., Saarikoski, S., Schnelle-Kreis, J., Surratt, J. D., Szidat, S., Szmigielski, R., and Wisthaler, A.: The molecular identification of organic compounds in the atmosphere: State of the art and challenges, Chem Rev, 115, 3919−3983, https://doi.org/10.1021/cr5003485, 2015.

O'Meara, S., Booth, A. M., Barley, M. H., Topping, D., and McFiggans, G.: An assessment of vapour pressure

800   estimation methods, Phys Chem Chem Phys, 16, 19453-19469, https://doi.org/10.1039/c4cp00857j, 2014.

Pankow, J. F., and Asher, W. E.: SIMPOL.1: a simple group contribution method for predicting vapor pressures and enthalpies of vaporization of multifunctional organic compounds, Atmos Chem Phys, 8, 2773–2796, https://doi.org/10.5194/acp-8-2773-2008, 2008.

805   Peräkylä, O., Riva, M., Heikkinen, L., Quelever, L., Roldin, P., and Ehn, M.: Experimental investigation into the volatilities of highly oxygenated organic molecules (HOMs), Atmos Chem Phys, 20, 649-669, https://doi.org/10.5194/acp-20-649-2020, 2020.

Pye, H. O., Luecken, D. J., Xu, L., Boyd, C. M., Ng, N. L., Baker, K. R., Ayres, B. R., Bash, J. O., Baumann, K., Carter, W. P., Edgerton, E., Fry, J. L., Hutzell, W. T., Schwede, D. B., and Shepson, P. B.: Modeling the Current and Future Roles of Particulate Organic Nitrates in the Southeastern United States, Environ Sci Technol, 49,
810   14195-14203, https://doi.org/10.1021/acs.est.5b03738, 2015.

Ren, S. M., Yao, L., Wang, Y. W., Yang, G., Liu, Y. L., Li, Y. Y., Lu, Y. Q., Wang, L. H., and Wang, L.: Volatility parameterization of ambient organic aerosols a a rural site of the North China Plain, Atmos Chem Phys, 22, 9283-9297, https://doi.org/10.5194/acp-22-9283-2022, 2022.

Riva, M., Rantala, P., Krechmer, J. E., Perakyla, O., Zhang, Y. J., Heikkinen, L., Garmash, O., Yan, C., Kulmala,
815   M., Worsnop, D., and Ehn, M.: Evaluating the performance of five different chemical ionization techniques for detecting gaseous oxygenated organic species, Atmos Meas Tech, 12, 2403–2421, https://doi.org/10.5194/amt-12-2403-2019, 2019.

Saarnio, K., Aurela, M., Timonen, H., Saarikoski, S., Teinila, K., Makela, T., Sofiev, M., Koskinen, J., Aalto, P. P., Kulmala, M., Kukkonen, J., and Hillamo, R.: Chemical composition of fine particles in fresh smoke plumes from
820   boreal wild-land fires in Europe, Sci Total Environ, 408, 2527-2542, https://doi.org/10.1016/j.scitotenv.2010.03.010, 2010.

Schobesberger, S., D'Ambro, E. L., Lopez-Hilfiker, F. D., Mohr, C., and Thornton, J. A.: A model framework to retrieve thermodynamic and kinetic properties of organic aerosol from composition-resolved thermal desorption measurements, Atmos Chem Phys, 18, 14757−14785, https://doi.org/10.5194/acp-18-14757-2018, 2018.

825   Shiraiwa, M., Ammann, M., Koop, T., and Pöschl, U.: Gas uptake and chemical aging of semisolid organic aerosol particles, P Natl Acad Sci USA, 108, 11003−11008, https://doi.org/10.1073/pnas.1103045108, 2011.

Stolzenburg, D., Fischer, L., Vogel, A. L., Heinritzi, M., Schervish, M., Simon, M., Wagner, A. C., Dada, L., Ahonen, L. R., Amorim, A., Baccarini, A., Bauer, P. S., Baumgartner, B., Bergen, A., Bianchi, F., Breitenlechner, M., Brilke, S., Mazon, S. B., Chen, D. X., Dias, A., Draper, D. C., Duplissy, J., Haddad, I., Finkenzeller, H., Frege, C.,
830   Fuchs, C., Garmash, O., Gordon, H., He, X., Helm, J., Hofbauer, V., Hoyle, C. R., Kim, C., Kirkby, J., Kontkanen, J., Kürten, A., Lampilahti, J., Lawler, M., Lehtipalo, K., Leiminger, M., Mai, H., Mathot, S., Mentler, B., Molteni, U., Nie, W., Nieminen, T., Nowak, J. B., Ojdanic, A., Onnela, A., Passananti, M., Petäjä, T., Quéléver, L. L. J., Rissanen, M. P., Sarnela, N., Schallhart, S., Tauber, C., Tomé, A., Wagner, R., Wang, M., Weitz, L., Wimmer, D., Xiao, M., Yan, C., Ye, P., Zha, Q., Baltensperger, U., Curtius, J., Dommen, J., Flagan, R. C., Kulmala, M., Smith,
835   J. N., Worsnop, D. R., Hansel, A., Donahue, N. M., and Winkler, P. M.: Rapid growth of organic aerosol nanoparticles over a wide tropospheric temperature range, P Natl Acad Sci USA, 115, 9122–9127, https://doi.org/10.1073/pnas.1807604115, 2018.

Thompson, S. L., Yatavelli, R. L. N., Stark, H., Kimmel, J. R., Krechmer, J. E., Day, D. A., Hu, W. W., Isaacman-VanWertz, G., Yee, L., Goldstein, A. H., Khan, M. A. H., Holzinger, R., Kreisberg, N., Lopez-Hilfiker, F. D.,
840   Mohr, C., Thornton, J. A., Jayne, J. T., Canagaratna, M., Worsnop, D. R., and Jimenez, J. L.: Field intercomparison of the gas/particle partitioning of oxygenated organics during the Southern Oxidant and Aerosol Study (SOAS) in 2013, Aerosol Sci Tech, 51, 30–56, https://doi.org/10.1080/02786826.2016.1254719, 2017.

Thornton, J. A., Mohr, C., Schobesberger, S., D'Ambro, E. L., Lee, B. H., and Lopez-Hilfiker, F. D.: Evaluating Organic Aerosol Sources and Evolution with a Combined Molecular Composition and Volatility Framework Using

845   the Filter Inlet for Gases and Aerosols (FIGAERO), Acc Chem Res, 53, 1415-1426, https://doi.org/10.1021/acs.accounts.0c00259, 2020.

Voliotis, A., Wang, Y., Shao, Y. Q., Du, M., Bannan, T. J., Percival, C. J., Pandis, S. N., Alfarra, M. R., and McFiggans, G.: Exploring the composition and volatility of secondary organic aerosols in mixed anthropogenic and biogenic precursor systems, Atmos Chem Phys, 21, 14251-14273, https://doi.org/10.5194/acp-21-14251-2021,
850   2021.

Wang, D. S., and Ruiz, L. H.: Chlorine-initiated oxidation of n-alkanes under high-NOx conditions: insights into secondary organic aerosol composition and volatility using a FIGAERO-CIMS, Atmos Chem Phys, 18, 15535−15553, https://doi.org/10.5194/acp-18-15535-2018, 2018.

Wang, M. Y., Chen, D. X., Xiao, M., Ye, Q., Stolzenburg, D., Hofbauer, V., Ye, P. L., Vogel, A. L., Mauldin III, R.
855   L., Amorim, A., Baccarini, A., Baumgartner, B., Brilke, S., Dada, L., Dias, A., Duplissy, J., Finkenzeller, H., Garmash, O., He, X. C., Hoyle, C. R., Kim, C., Kvashnin, A., Lehtipalo, K., Fischer, L., Molteni, U., Petäjä, T., Pospisilova, V., Quéléver, L. L. J., Rissanen, M., Simon, M., Tauber, C., Tomé, A., Wagner, A. C., Weitz, L., Volkamer, R., Winkler, P. M., Kirkby, J., Worsnop, D. R., Kulmala, M., Baltensperger, U., Dommen, J., El-Haddad, I., and Donahue, N. M.: Photo-oxidation of aromatic hydrocarbons produces low-volatility organic
860   compounds, Environ Sci Technol, 54, 7911–7921, https://doi.org/10.1021/acs.est.0c02100, 2020.

Wu, C., Bell, D., Graham, E. L., Haslett, S., Riipinen, I., Baltensperger, U., Bertrand, A., Giannoukos, S., Schoonbaert, J., El Haddad, I., Prevot, A. S. H., Huang, W., and Mohr, C.: Photolytically Induced Changes in Composition and Volatility of Biogenic Secondary Organic Aerosol from Nitrate Radical Oxidation during Night-to-day Transition, Atmos Chem Phys Discuss, 1-29, https://doi.org/10.5194/acp-2021-347, 2021.

865   Yang, L. H., Takeuchi, M., Chen, Y. L., and Ng, N. L.: Characterization of thermal decomposition of oxygenated organic compounds in FIGAERO-CIMS, Aerosol Sci Tech, 55, 1321-1342, https://doi.org/10.1080/02786826.2021.1945529, 2021.

Yli-Juuti, T., Pajunoja, A., Tikkanen, O.-P., Buchholz, A., Faiola, C., Väisänen, O., Hao, L., Kari, E., Peräkylä, O., Garmash, O., Shiraiwa, M., Ehn, M., Lehtinen, K., and Virtanen, A.: Factors controlling the evaporation of
870   secondary organic aerosol from α-pinene ozonolysis, Geophys Res Lett, 44, 2562−2570, https://doi.org/10.1002/2016GL072364, 2017.

Ylisirniö, A., Barreira, L. M. F., Pullinen, I., Buchholz, A., Jayne, J., Krechmer, J. E., Worsnop, D. R., Virtanen, A., and Schobesberger, S.: On the calibration of FIGAERO-ToF-CIMS: importance and impact of calibrant delivery for the particle-phase calibration, Atmos Meas Tech, 14, 355–367, https://doi.org/10.5194/amt-14-355-2021, 2021.

875   Zha, Q., Aliaga, D., Krejci, R., Sinclair, V. A., Wu, C., Ciarelli, G., Scholz, W., Heikkinen, L., Partoll, E., Gramlich, Y., Huang, W., Leiminger, M., Enroth, J., Peräkylä, O., Cai, R., Chen, X., Koenig, A. M., Velarde, F., Moreno, I., Petäjä, T., Artaxo, P., Laj, P., Hansel, A., Carbone, C., Kulmala, M., Andrade, M., Worsnop, D., Mohr, C., and Bianchi, F.: Oxidized organic molecules in the tropical free troposphere over Amazonia, National Science Review, nwad138, https://doi.org/10.1093/nsr/nwad138, 2023a.

880   Zha, Q. Z., Huang, W., Aliaga, D., Perakyla, O., Heikkinen, L., Koenig, A. M., Wu, C., Enroth, J., Gramlich, Y., Cai, J., Carbone, S., Hansel, A., Petaja, T., Kulmala, M., Worsnop, D., Sinclair, V., Krejci, R., Andrade, M., Mohr, C., and Bianchi, F.: Measurement report: Molecular-level investigation of atmospheric cluster ions at the tropical high-altitude research station Chacaltaya (5240 m a.s.l.) in the Bolivian Andes, Atmos Chem Phys, 23, 4559-4576, https://doi.org/10.5194/acp-23-4559-2023, 2023b.

885 Zhang, H. F., Yee, L. D., Lee, B. H., Curtis, M. P., Worton, D. R., Isaacman-VanWertz, G., Offenberg, J. H.,
Lewandowski, M., Kleindienst, T. E., Beaver, M. R., Holder, A. L., Lonneman, W. A., Docherty, K. S., Jaoui, M.,
Pye, H. O. T., Hu, W. W., Day, D. A., Campuzano-Jost, P., Jimenez, J. L., Guo, H. Y., Weber, R. J., de Gouw, J.,
Koss, A. R., Edgerton, E. S., Brune, W., Mohr, C., Lopez-Hilfiker, F. D., Lutz, A., Kreisberg, N. M., Spielman, S.
R., Hering, S. V., Wilson, K. R., Thornton, J. A., and Goldstein, A. H.: Monoterpenes are the largest source of
890 summertime organic aerosol in the southeastern United States, P Natl Acad Sci USA, 115, 2038–2043,
https://doi.org/10.1073/pnas.1717513115, 2018.

Zheng, X., Wu, Y., Zhang, S., Hu, J., Zhang, K. M., Li, Z., He, L., and Hao, J.: Characterizing particulate polycyclic
aromatic hydrocarbon emissions from diesel vehicles using a portable emissions measurement system, Sci Rep-
Uk, 7, 10058, https://doi.org/10.1038/s41598-017-09822-w, 2017.

895